Front. Optoelectron. 2017, 10(2): 103–110
DOI 10.1007/s12200-017-0716-6

RESEARCH ARTICLE

Hole-transporting layer-free inverted planar mixed lead-tin perovskite-based solar cells

Yuqin LIAO[1,2,3*], Xianyuan JIANG[2,3*], Wenjia ZHOU[2], Zhifang SHI[2,3], Binghan LI[2,3], Qixi MI[2], Zhijun NING (✉)[2]

1 Shanghai Institute of Microsystem and Information Technology, Chinese Academy of Sciences, Shanghai 200050, China
2 School of Physical Science and Technology, ShanghaiTech University, Shanghai 201210, China
3 University of Chinese Academy of Sciences, Beijing 100049, China

Abstract Mixed lead-tin (Pb-Sn) perovskites present a promising strategy to extend the light-harvesting range of perovskite-based solar cells (PSCs). The use of electron-transporting layer or hole-transporting layer (HTL) is critical to achieve high device efficiency. This strategy, however, requires tedious layer-by-layer fabrication as well as high-temperature annealing for certain oxides. In this work, we fabricated HTL-free planar $FAPb_{0.5}Sn_{0.5}I_3$ PSCs with the highest efficiency of 7.94%. High short-circuit current density of 23.13 mA/cm^2 was attained, indicating effective charge extraction at the ITO/$FAPb_{0.5}Sn_{0.5}I_3$ interface. This finding provides an alternative strategy to simplify the manufacture of single-junction or tandem PSCs.

Keywords solar cell, perovskite, hole-transporting layer (HTL), interface engineering

1 Introduction

Organic–inorganic hybrid halide perovskite-based solar cells (PSCs) received tremendous attention in recent years owing to its high absorption coefficient, small exciton-binding energy, high carrier mobility, and extensive carrier-diffusion lengths [1–9]. Single-junction PSCs have achieved a power conversion efficiency (PCE) of 22.1% [10–14]. Tandem solar cells present a promising strategy to further enhance device performance due to the Shockley-Queisser limit for single-junction devices [15,16]. With its proper small band gap (E_g) of 0.9 to 1.2 eV, mixed lead-tin (Pb-Sn) perovskite is an ideal light-harvesting material for rear cell in tandem solar cells. Recently, PSCs based on a mixed Pb-Sn perovskite-based absorber with an efficiency of 17% have been demonstrated [17].

Two device architectures are commonly used for PSCs: the conventional n-i-p structure and the inverted p-i-n structure. In both structures, a perovskite active layer is sandwiched between a hole-transporting layer (HTL) and an electron-transporting layer (ETL). For conventional n-i-p structures, the most frequently used ETLs are transition metal oxides (TiO_2 and ZnO), whereas HTLs are mainly organic materials, such as 2,2′,7,7′-tetrakis [*N*,*N*-di(4-methoxyphenyl) amino]-9,9′-spirobifluorene (spiro-OMeTAD) [18–21]. Inverted devices generally employ NiO_x, poly(3,4-ethylenedioxythiophene) polystyrene sulfonate (PEDOT: PSS) as HTL, and [6,6]-phenyl C61-butyric acid methyl ester (PCBM), ZnO, or SnO_2 as the top ETL [22–25]. For inverted device structures, both ETL and HTL can use inorganic materials, thus facilitating better device stability. Numerous studies have attempted to optimize the contact between the active layer and the carrier-transporting layers, as well as between the carrier-transporting layers and the electrodes, to achieve quick carrier transport and less interface recombination [26–30]. Given the tedious device-fabrication process for each layer (especially the requirement of high-temperature annealing process for the fabrication of some oxide films), ETL- or HTL-free devices were developed to simplify device fabrication [26,31–37]. HTL-free inverted-structure solar cells based on both Pb and Sn perovskites have been reported with good performance and stability [34–38].

In the current work, we constructed an HTL-free planar Pb-Sn binary PSC by preparing perovskite film on bare indium tin oxide (ITO) for the first time. Homogeneous and mirror-like $FAPb_{0.5}Sn_{0.5}I_3$ films were developed

Received March 28, 2017; accepted April 7, 2017

E-mail: ningzhj@shanghaitech.edu.cn

*These authors contributed equally to this work.

through anti-solvent assisted crystallization and solvent engineering. The effect of the Pb-Sn ratio as well as the concentration of SnF_2 on film morphology and device performance were investigated. Based on the inverted-structure (ITO/perovskite/PCBM/BCP/Al), solar cells with a highest PCE of 7.94% under the illumination of AM 1.5G solar simulator were presented.

2 Experimental section

2.1 Perovskite precursor preparation

The perovskite precursor solution was obtained by mixing the solutions of $FASnI_3$ and $FAPbI_3$ at a specific ratio. $FASnI_3$ and $FAPbI_3$ solutions of 1-M[1)] concentration were prepared in a mixed solvent of *N*,*N*-dimethylformamide (DMF) and dimethyl sulfoxide (DMSO) (volume ratio of 3:2). The mole ratio of FAI to SnI_2/PbI_2 was 1:1. Furthermore, 0.1 M SnF_2 was added to the tin precursor to prevent oxidation of the Sn^{2+} to Sn^{4+} unless otherwise stated. The final solution was stirred at 70°C for 1 h and subsequently filtered with a PTFE filter (0.22 μm pore size) before use.

2.2 Perovskite film fabrication

For $FAPb_{1-x}Sn_xI_3$ film ($x > 0.25$) fabrication, the mixed precursor prepared above was spin coated onto the substrate via a one-step anti-solvent assisted crystalline process at 1000 and 5000 rpm for 10 and 30 s, respectively. In the second process, 800 μL toluene was slowly dropped in the middle of the substrate. The perovskite film was subsequently annealed at 70°C for 30 min.

For $FAPbI_3$ and $FAPb_{0.75}Sn_{0.25}I_3$ films, the annealing temperature was increased to 170°C and 100°C, respectively. All of the operations were performed in a glovebox ($O_2 \leqslant 1$ ppm, $H_2O \leqslant 1$ ppm).

2.3 Device fabrication

ITO-coated glasses were sequentially cleaned with Triton X-100 detergent, acetone, deionized water, and isopropanol. The cleaned ITO glasses were treated with UVO for 3 min before being transferred into the glovebox. Perovskites were fabricated on top of the ITO glasses using the procedure described above. The PCBM film was prepared via a spin-coating process (speed of 2000 rpm and time of 60 s) using chlorobenzene as the solvent (concentration of 10 mg/mL), followed by annealing at 80°C for 5 min. Subsequently, a saturated solution of BCP in anhydrous methanol was spin coated at 6000 rpm for 15 s. Aluminum (of 100 nm thickness) was thermally evaporated as the top electrode at a rate of 1 Å/s.

2.4 Device characterization

Current-voltage (*J-V*) curves were measured using a Keithley 2400 source unit under AM1.5G solar simulator (Enli Tech, Taiwan) at 100 mW/cm^2 (1 sun). The light intensity was calibrated by a certified KG-5 Si diode. The spectral mismatch correction factor is 0.49%. The devices were measured in reverse scan (from 0.7 to 0 V, at increments of 0.01 V) and the delay time was 30 ms. *J-V* curves for all devices were measured by masking the active area using a metal mask with an area of 0.04 cm^2. The external quantum efficiency (EQE) spectra were obtained by a commercial system (Solar Cell Scan 100, Beijing Zolix Instruments Co., Ltd). Additionally, the cells were subjected to monochromatic illumination (150 W Xe lamp passing through monochromator filters). The light intensity was calibrated by a standard photodetector (QE-B3/S1337-1010BQ, Zolix). The light beam was chopped at 180 Hz, and the response of the cell was acquired using a Stanford Research SR830 lock-in amplifier.

3 Results and discussion

We firstly investigated the optical properties of the mixed Pb-Sn perovskites. As the Sn is added, the absorption spectra of $FAPb_{1-x}Sn_xI_3$ (x = 0.25, 0.50, 0.75, 1.00) are all red shifted. Based on the absorption onset point, the band gaps of $FAPb_{0.75}Sn_{0.25}I_3$ and $FAPb_{0.5}Sn_{0.5}I_3$ are estimated to be 1.31 and 1.27 eV, respectively (Fig. 1(a)). The absorption tail mainly results from sub-band gap states [39]. Photoluminescence (PL) spectra show similar trend as the absorption spectra (Fig. 1(b)). The E_g values estimated from both absorption and PL are shown in Table 1. As the Sn content increases from 0% to 75%, the estimated E_g decreases from 1.507 to 1.282 eV, and recovers to 1.40 eV for $FASnI_3$. The small band gaps of mixed Pb-Sn perovskites can be attributed to the synergistic effect of the relatively higher valence band

Table 1 Band gaps for Pb-Sn perovskite alloys calculated from absorption edge and PL peak, respectively

$FAPb_{1-x}Sn_xI_3$	0	0.25	0.50	0.75	1.00
band gap from absorption/eV	1.490	1.310	1.270	–	–
band gap from PL/eV	1.507	1.355	1.286	1.282	1.400

1) 1 M = 1 mol/L

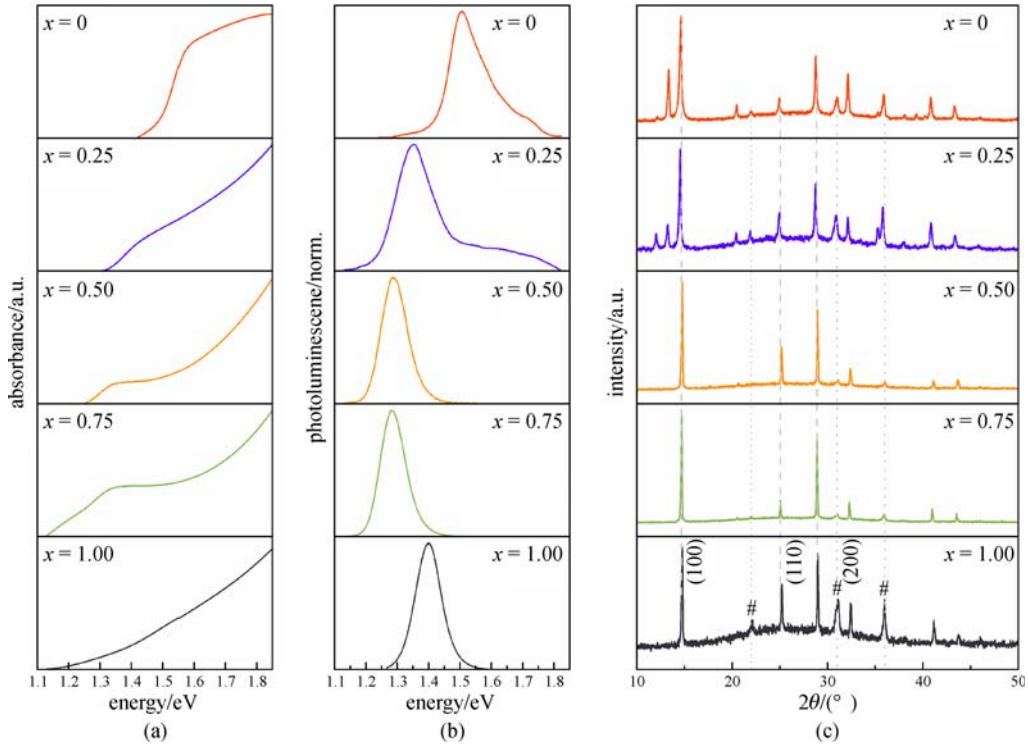

Fig. 1 Optical and structural characterization of $FAPb_{1-x}Sn_xI_3$. (a) Absorption spectra; (b) photoluminescence spectra; and (c) X-ray diffraction (XRD) patterns of $FAPb_{1-x}Sn_xI_3$ films with different Sn ratios; "#" indicates the diffraction peaks of ITO

maximum of Sn and lower conduction band minimum of Pb. The multi-PL peaks of $FAPbI_3$ and $FAPb_{0.75}Sn_{0.25}I_3$ films were ascribed to phase impurity.

XRD experiment was conducted to study the structure of $FAPb_{1-x}Sn_xI_3$ films (Fig. 1(c)). All of the samples show diffraction peaks near 14°, 25°, and 28°, corresponding to the (100), (110), and (200) planes of the cubic structure of $FAPb_{1-x}Sn_xI_3$. High-temperature post-annealing was employed to convert $FAPbI_3$ and $FAPb_{0.75}Sn_{0.25}I_3$ to cubic structure. $FAPbI_3$ and $FAPb_{0.75}Sn_{0.25}I_3$ films show extra diffraction peaks corresponding to a triclinic structure (Fig. S1), possibly deriving from the high formation energy of a cubic structure, despite the high-temperature post-annealing employed to convert $FAPbI_3$ and $FAPb_{0.75}Sn_{0.25}I_3$ to a cubic structure. As the Sn content increased, the extra peaks disappeared, while a pure cubic structure was observed. We conclude that the addition of Sn reduced the formation energy of the cubic phase [40].

Given its uniform crystal structure and extended absorption range, we explored $FAPb_{0.5}Sn_{0.5}I_3$ films as a light absorber for solar cells based on inverted planar architecture: ITO/perovskite/PCBM/BCP/Al (Fig. 2(a)). In this study, PCBM and BCP serve as the ETL and HTL. According to the cross-sectional scanning electron microscopy (SEM) image (Fig. 2(b)), the thickness of the $FAPb_{0.5}Sn_{0.5}I_3$, PCBM, and BCP films are approximately 270, 55, and 45 nm, respectively. Figure 2(c) shows the band alignment diagram of the HTL-free devices. The conduction band and valence band position are estimated to be 4.00 and 5.25 eV, respectively [40]. The small difference between the work function of ITO and the valence band of the perovskite allows for effective hole injection. As shown in Fig. 2(d), our champion cell with 10% (molar ratio) SnF_2 achieves a maximum PCE of 7.94%, with an open-circuit voltage (V_{oc}) of 0.59 V, a short-circuit current density (J_{sc}) of 23.13 mA/cm^2, and a fill factor (*FF*) of 58%.

From the EQE spectra, the solar cells based on mixed Pb-Sn perovskite exhibit high EQE in a broad absorption range of up to 1050 nm (Fig. 2(e)), and the highest EQE reaches 80.4% at 520 nm. The integrated J_{sc} from the EQE spectrum (22.57 mA/cm^2) matches well with the J_{sc} obtained in *J-V* curves measured under solar simulator (with a difference within ±3%). This high J_{sc} demonstrates that holes can be effectively collected by ITO without the HTL. We subsequently investigated the stability of the devices under continuous simulated AM 1.5G illumination (Fig. S2), in a N_2-filled glovebox with $O_2 < 2$ ppm, $H_2O < 1$ ppm. Device efficiency slightly increased initially, and then remained steady. The illumination-initiated improvement of efficiency can be ascribed to the drift of ions in perovskites driven by photovoltage-induced electric field, forming an *in situ* p-i-n homojunction [41].

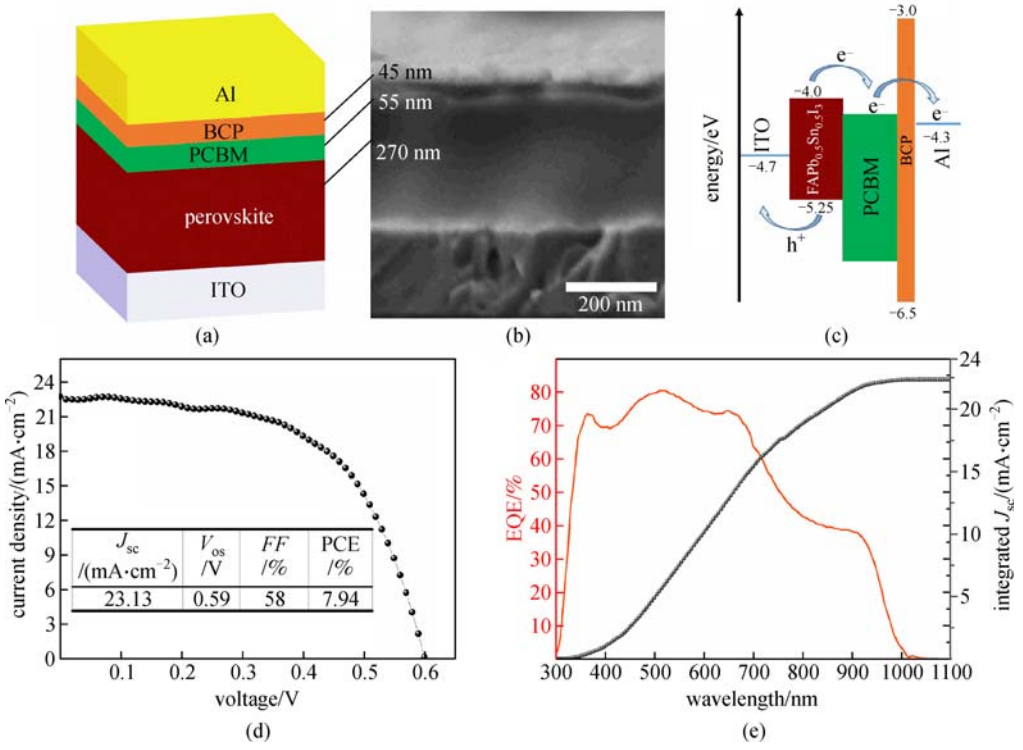

Fig. 2 Photovoltaic structure and performance of HTL-free devices based on $FAPb_{0.5}Sn_{0.5}I_3$ films. (a) Schematics of the device architecture; (b) SEM cross-sectional image; (c) energy band diagram; (d) *J-V* characteristics; (e) EQE spectrum and integrated J_{sc} of the highest performance of HTL-free PSC

To investigate the impact of the energy-level alignment between ITO and perovskite, we prepared a control sample using NiO_x as an HTL (Fig. S3). The XRD patterns of perovskite films prepared on ITO and NiO_x substrates exhibited similar cubic structures and good crystallinity (see Fig. 3(a)). The J_{sc} and *FF* of the PSC with NiO_x as HTL, however, are significantly lower compared with the HTL-free one. This condition may result from the deep work function of NiO_x, which affected the hole transfer from perovskite. To confirm this speculation, we examined the PL spectra of $FAPb_{0.5}Sn_{0.5}I_3$ films on ITO and NiO_x. As illustrated in Fig. 3(b), the emission intensity at 964 nm of the film on ITO is significantly weaker, implying worse hole transport between NiO_x/$FAPb_{0.5}Sn_{0.5}I_3$. We further compared the perovskite film morphology through SEM, as shown in Fig. 3(c). The $FAPb_{0.5}Sn_{0.5}I_3$ film exhibits higher surface coverage and larger crystal domain size on bare ITO (left). More pinholes and smaller grains appear when NiO_x (right) was employed, which would lead to direct contact between NiO_x and ETL and severe interface charge recombination.

SnF_2 is generally employed to stabilize the $FASnI_3$ perovskites from oxidation owing to its reducing character [42,43]. The addition of excess amount of SnF_2, however, will induce phase separation of the film, thus generating poor device performance [42,43]. We systematically investigated the impact of SnF_2 molar concentration on film morphology and device performance. As shown in Figs. 4(a)–4(e), pure $FAPb_{0.5}Sn_{0.5}I_3$ exhibits a full coverage and small grain size. Larger grain size along with pinholes appeared when 5 mol% SnF_2 was added. Upon adding 10 mol% of SnF_2, rock-like grains with large domain size emerged with a relatively high coverage ratio. When more SnF_2 was incorporated, both grain size and coverage rate decreased. The maximum value of the average grain size was around 280 nm with SnF_2 ratio of 10 mol% (Fig. 4(f)). We further compared the Sn^{4+} content in the $FAPb_{0.5}Sn_{0.5}I_3$ films with or without SnF_2 additive using X-ray photoelectron spectroscopy. To exclude the effect of surface oxidation, samples were etched before the measurement (Fig. S4 and Table S1). As shown in Table S1, the Sn^{4+} amount in the 10 mol% SnF_2-doped $FAPb_{0.5}Sn_{0.5}I_3$ film is significantly lower than that in pure $FAPb_{0.5}Sn_{0.5}I_3$, implying that the addition of SnF_2 prevents Sn^{2+} from oxidation.

The PSCs based on $FAPb_{0.5}Sn_{0.5}I_3$ with various molar concentrations of SnF_2 were fabricated. As shown in Fig. S5 and Table S2, the devices exhibited low J_{sc} and efficiency without SnF_2 additives. This condition can be attributed to the high defect density resulting from the oxidation of Sn^{2+} to Sn^{4+}, causing significantly reduced carrier-diffusion lengths [42–44]. With the addition of

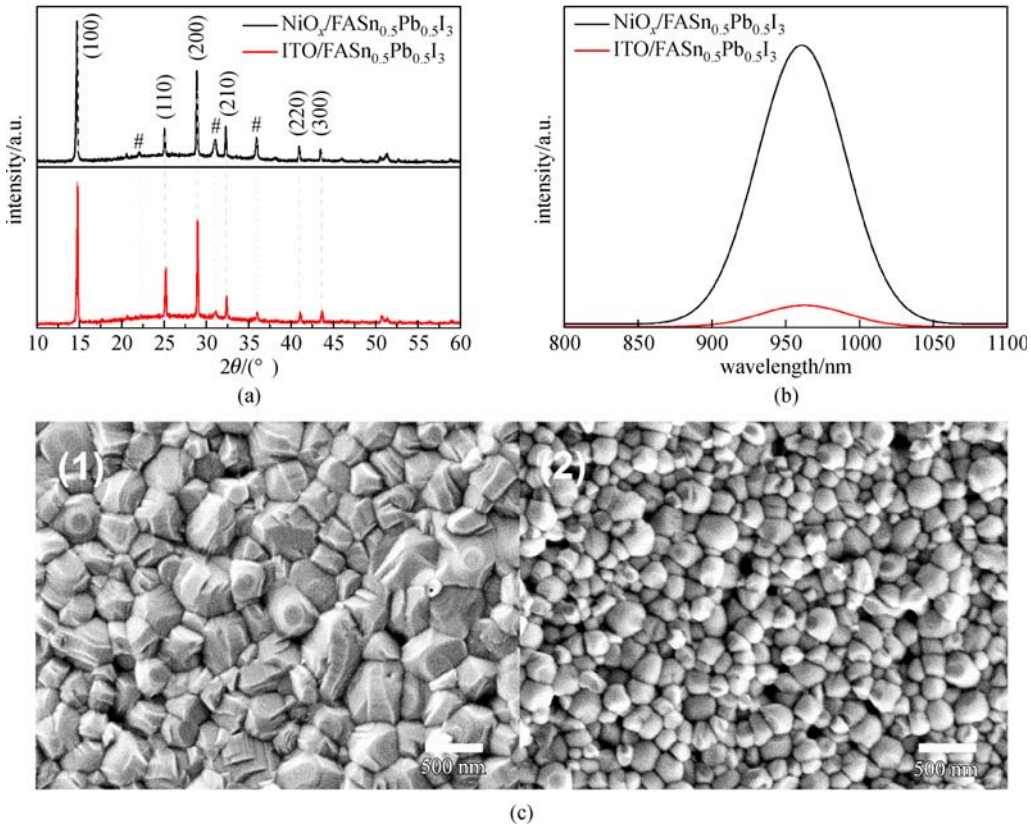

Fig. 3 Characterizations of $FAPb_{0.5}Sn_{0.5}I_3$ films on different substrates. (a) XRD patterns ("#" indicates the diffraction peaks of ITO); (b) PL spectra; and (c) SEM images of the perovskite film on ITO and NiO_x

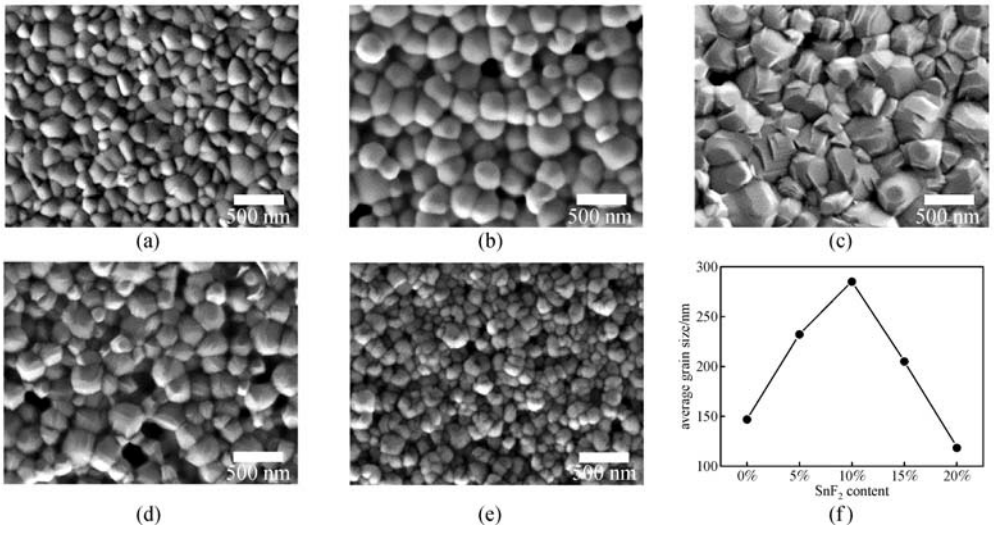

Fig. 4 Morphology of perovskite films with varying molar concentration of SnF_2. SEM images of $FAPb_{0.5}Sn_{0.5}I_3$ films on ITO with (a) 0 mol%, (b) 5 mol% , (c) 10 mol%, (d) 15 mol%, and (e) 20 mol% of SnF_2; and (f) calculation of the average grain size for perovskites

SnF_2, the device performance is effectively improved by suppressing Sn oxidation. However, film morphology deteriorated when the concentration of SnF_2 is increased to 20%, leading to poor performance. Therefore, both oxidation and film morphology are important to device performance.

4 Conclusion

In this study, we constructed an inverted planar mixed Pb-Sn perovskite solar cell on bare ITO glass without an independent HTL. The Pb-to-Sn ratio and the concentration of SnF_2 were systematically optimized. Highly uniform reflective $FAPb_{0.5}Sn_{0.5}I_3$ thin films on ITO glass with a band gap of 1.28 eV were achieved. Solar cells based on HTL-free ITO/$FAPb_{0.5}Sn_{0.5}I_3$/PCBM/BCP/Al structure exhibit a promising PCE of 7.94% with a short-circuit current density of 23.13 mA/cm^2, EQE of 80%, and extended light-harvesting range to 1050 nm. The removal of HTL allows effective carrier transfer between the perovskite and the ITO electrode. It therefore provides an alternative simple structure for low-temperature, small band gap single-junction or tandem PSCs.

Acknowledgements This work was supported by start-up funding from ShanghaiTech University, The Young 1000 Talents Program, the National Natural Science Foundation of China (Grant Nos. U1632118, and 21571129), the National Key Research Program (No. 2016YFA0204000), the Shanghai Key Research Program (No. 16JC1402100), and the Shanghai International Cooperation Project (No. 16520720700). The authors are grateful to the test centers of both ShanghaiTech University and CAS Key Laboratory of Low-Carbon Conversion Science and Engineering, Shanghai Advanced Research Institute, Chinese Academy of Sciences.

References

1. Sun S, Salim T, Mathews N, Duchamp M, Boothroyd C, Xing G, Sum T C, Lam Y M. The origin of high efficiency in low-temperature solution-processable bilayer organometal halide hybrid solar cells. Energy & Environmental Science, 2014, 7(1): 399–407
2. Park N G. Perovskite solar cells: an emerging photovoltaic technology. Materials Today, 2015, 18(2): 65–72
3. Ishihara T. Optical properties of PbI-based perovskite structures. Journal of Luminescence, 1994, 60–61: 269–274
4. Zhang W, Saliba M, Stranks S D, Sun Y, Shi X, Wiesner U, Snaith H J. Enhancement of perovskite-based solar cells employing core-shell metal nanoparticles. Nano Letters, 2013, 13(9): 4505–4510
5. Wehrenfennig C, Eperon G E, Johnston M B, Snaith H J, Herz L M. High charge carrier mobilities and lifetimes in organolead trihalide perovskites. Advanced Materials, 2014, 26(10): 1584–1589
6. Ponseca C S Jr, Savenije T J, Abdellah M, Zheng K, Yartsev A, Pascher T, Harlang T, Chabera P, Pullerits T, Stepanov A, Wolf J P, Sundström V. Organometal halide perovskite solar cell materials rationalized: ultrafast charge generation, high and microsecond-long balanced mobilities, and slow recombination. Journal of the American Chemical Society, 2014, 136(14): 5189–5192
7. Stranks S D, Eperon G E, Grancini G, Menelaou C, Alcocer M J P, Leijtens T, Herz L M, Petrozza A, Snaith H J. Electron-hole diffusion lengths exceeding 1 micrometer in an organometal trihalide perovskite absorber. Science, 2013, 342(6156): 341–344
8. Xing G, Mathews N, Sun S, Lim S S, Lam Y M, Grätzel M, Mhaisalkar S, Sum T C. Long-range balanced electron- and hole-transport lengths in organic-inorganic $CH_3NH_3PbI_3$. Science, 2013, 342(6156): 344–347
9. Dong Q, Fang Y, Shao Y, Mulligan P, Qiu J, Cao L, Huang J. Electron-hole diffusion lengths > 175 μm in solution-grown $CH_3NH_3PbI_3$ single crystals. Science, 2015, 347(6225): 967–970
10. Green M A, Ho-Baillie A, Snaith H J. The emergence of perovskite solar cells. Nature Photonics, 2014, 8(7): 506–514
11. Snaith H J. Perovskites: the emergence of a new era for low-cost, high-efficiency solar cells. Journal of Physical Chemistry Letters, 2013, 4(21): 3623–3630
12. Liu M, Johnston M B, Snaith H J. Efficient planar heterojunction perovskite solar cells by vapour deposition. Nature, 2013, 501 (7467): 395–398
13. Kojima A, Teshima K, Shirai Y, Miyasaka T. Organometal halide perovskites as visible-light sensitizers for photovoltaic cells. Journal of the American Chemical Society, 2009, 131(17): 6050–6051
14. Solar cell efficiency table, www.nrel.gov/ncpv/; accessed: April 2016
15. Yang W S, Noh J H, Jeon N J, Kim Y C, Ryu S, Seo J, Seok S I. High-performance photovoltaic perovskite layers fabricated through intramolecular exchange. Science, 2015, 348(6240): 1234–1237
16. Shockley W, Queisser H J. Detailed balance limit of efficiency of p-n junction solar cells. Journal of Applied Physics, 1961, 32(3): 510–519
17. Zhao D, Yu Y, Wang C, Liao W, Shrestha N, Grice C R, Cimaroli A J, Guan L, Ellingson R J, Zhu K, Zhao X, Xiong R G, Yan Y. Low-bandgap mixed tin–lead iodide perovskite absorbers with long carrier lifetimes for all-perovskite tandem solar cells. Nature Energy, 2017, 2: 17018
18. Lee M M, Teuscher J, Miyasaka T, Murakami T N, Snaith H J. Efficient hybrid solar cells based on meso-superstructured organo-metal halide perovskites. Science, 2012, 338(6107): 643–647
19. Eperon G E, Burlakov V M, Docampo P, Goriely A, Snaith H J. Morphological control for high performance, solution-processed planar heterojunction perovskite solar cells. Advanced Functional Materials, 2014, 24(1): 151–157
20. Liu D, Kelly T L. Perovskite solar cells with a planar heterojunction structure prepared using room-temperature solution processing techniques. Nature Photonics, 2013, 8(2): 133–138
21. Zhou H, Chen Q, Li G, Luo S, Song T B, Duan H S, Hong Z, You J, Liu Y, Yang Y. Interface engineering of highly efficient perovskite solar cells. Science, 2014, 345(6196): 542–546
22. Jeng J Y, Chiang Y F, Lee M H, Peng S R, Guo T F, Chen P, Wen T C. $CH_3NH_3PbI_3$ perovskite/fullerene planar-heterojunction hybrid solar cells. Advanced Materials, 2013, 25(27): 3727–3732
23. Nie W, Tsai H, Asadpour R, Blancon J C, Neukirch A J, Gupta G, Crochet J J, Chhowalla M, Tretiak S, Alam M A, Wang H L, Mohite A D. High-efficiency solution-processed perovskite solar cells with millimeter-scale grains. Science, 2015, 347(6221): 522–525
24. Heo J H, Han H J, Kim D, Ahn T K, Im S H. Hysteresis-less inverted $CH_3NH_3PbI_3$ planar perovskite hybrid solar cells with 18.1% power conversion efficiency. Energy & Environmental Science, 2015, 8(5): 1602–1608
25. Wang J T W, Wang Z, Pathak S, Zhang W, deQuilettes D W, Wisnivesky-Rocca-Rivarola F, Huang J, Nayak P K, Patel J B,

Mohd Yusof H A, Vaynzof Y, Zhu R, Ramirez I, Zhang J, Ducati C, Grovenor C, Johnston M B, Ginger D S, Nicholas R J, Snaith H J. Efficient perovskite solar cells by metal ion doping. Energy & Environmental Science, 2016, 9(9): 2892–2901

26. Liu L, Mei A, Liu T, Jiang P, Sheng Y, Zhang L, Han H. Fully printable mesoscopic perovskite solar cells with organic silane self-assembled monolayer. Journal of the American Chemical Society, 2015, 137(5): 1790–1793
27. Yang Y, Ri K, Mei A, Liu L, Hu M, Liu T, Li X, Han H. The size effect of TiO_2 nanoparticles on a printable mesoscopic perovskite solar cell. Journal of Materials Chemistry A, Materials for Energy and Sustainability, 2015, 3(17): 9103–9107
28. Luo Q, Ma H, Zhang Y, Yin X, Yao Z, Wang N, Li J, Fan S, Jiang K, Lin H. Cross-stacked superaligned carbon nanotube electrodes for efficient hole conductor-free perovskite solar cells. Journal of Materials Chemistry A, Materials for Energy and Sustainability, 2016, 4(15): 5569–5577
29. Yang Y, Xiao J, Wei H, Zhu L, Li D, Luo Y, Wu H, Meng Q. An all-carbon counter electrode for highly efficient hole-conductor-free organo-metal perovskite solar cells. RSC Advances, 2014, 4(95): 52825–52830
30. Yu Z, Chen B, Liu P, Wang C, Bu C, Cheng N, Bai S, Yan Y, Zhao X. Stable organic-inorganic perovskite solar cells without hole-conductor layer achieved via cell structure design and contact engineering. Advanced Functional Materials, 2016, 26(27): 4866–4873
31. Ye S, Rao H, Yan W, Li Y, Sun W, Peng H, Liu Z, Bian Z, Li Y, Huang C. A strategy to simplify the preparation process of perovskite solar cells by Co-deposition of a hole-conductor and a perovskite layer. Advanced Materials, 2016, 28(43): 9648–9654
32. Hu Q, Wu J, Jiang C, Liu T, Que X, Zhu R, Gong Q. Engineering of electron-selective contact for perovskite solar cells with efficiency exceeding 15%. ACS Nano, 2014, 8(10): 10161–10167
33. Mei A, Li X, Liu L, Ku Z, Liu T, Rong Y, Xu M, Hu M, Chen J, Yang Y, Grätzel M, Han H. A hole-conductor-free, fully printable mesoscopic perovskite solar cell with high stability. Science, 2014, 345(6194): 295–298
34. Tsai K W, Chueh C C, Williams S T, Wen T C, Jen A K Y. High-performance hole-transporting layer-free conventional perovskite/fullerene heterojunction thin-film solar cells. Journal of Materials Chemistry A, Materials for Energy and Sustainability, 2015, 3(17): 9128–9132
35. Li Y, Ye S, Sun W, Yan W, Li Y, Bian Z, Liu Z, Wang S, Huang C. Hole-conductor-free planar perovskite solar cells with 16.0% efficiency. Journal of Materials Chemistry A, Materials for Energy and Sustainability, 2015, 3(36): 18389–18394
36. Bao X, Zhu Q, Qiu M, Yang A, Wang Y, Zhu D, Wang J, Yang R. High-performance inverted planar perovskite solar cells without a hole transport layer via a solution process under ambient conditions. Journal of Materials Chemistry A, Materials for Energy and Sustainability, 2015, 3(38): 19294–19298
37. Zhang Y, Hu X, Chen L, Huang Z, Fu Q, Liu Y, Zhang L, Chen Y. Flexible, hole transporting layer-free and stable $CH_3NH_3PbI_3$/$PC_{61}BM$ planar heterojunction perovskite solar cells. Organic Electronics, 2016, 30: 281–288
38. Marshall K P, Walker M, Walton R I, Hatton R A. Enhanced stability and efficiency in hole-transport-layer-free CsSnI3 perovskite photovoltaics. Nature Energy, 2016, 1: 16178
39. Feng H J, Paudel T R, Tsymbal E Y, Zeng X C. Tunable optical properties and charge separation in $CH_3NH_3Sn_xPb_{1-x}I_3/TiO_2$-based planar perovskites cells. Journal of the American Chemical Society, 2015, 137(25): 8227–8236
40. Eperon G E, Leijtens T, Bush K A, Prasanna R, Green T, Wang J T W, McMeekin D P, Volonakis G, Milot R L, May R, Palmstrom A, Slotcavage D J, Belisle R A, Patel J B, Parrott E S, Sutton R J, Ma W, Moghadam F, Conings B, Babayigit A, Boyen H G, Bent S, Giustino F, Herz L M, Johnston M B, McGehee M D, Snaith H J. Perovskite-perovskite tandem photovoltaics with optimized band gaps. Science, 2016, 354(6314): 861–865
41. Deng Y, Xiao Z, Huang J. Light-induced self-poling effect on organometal trihalide perovskite solar cells for increased device efficiency and stability. Advanced Energy Materials, 2015, 5(20): 1500721
42. Kumar M H, Dharani S, Leong W L, Boix P P, Prabhakar R R, Baikie T, Shi C, Ding H, Ramesh R, Asta M, Graetzel M, Mhaisalkar S G, Mathews N. Lead-free halide perovskite solar cells with high photocurrents realized through vacancy modulation. Advanced Materials, 2014, 26(41): 7122–7127
43. Koh T M, Krishnamoorthy T, Yantara N, Shi C, Leong W L, Boix P P, Grimsdale A C, Mhaisalkar S G, Mathews N. Formamidinium tin-based perovskite with low E_g for photovoltaic applications. Journal of Materials Chemistry A, Materials for Energy and Sustainability, 2015, 3(29): 14996–15000
44. Liao W, Zhao D, Yu Y, Grice C R, Wang C, Cimaroli A J, Schulz P, Meng W, Zhu K, Xiong R G, Yan Y. Lead-free inverted planar formamidinium tin triiodide perovskite solar cells achieving power conversion efficiencies up to 6.22. Advanced Materials, 2016, 28 (42): 9333–9340

Yuqin Liao is a Master degree candidate in the School of Physical Science and Technology, ShanghaiTech University under the supervision of Prof. Zhijun Ning. She received her B.E. degree in the School of Materials Science and Engineering, Huazhong University of Science and Technology in 2014. Her research interests include the design and application of tin-based perovskite materials for photovoltaics.

Xianyuan Jiang is a graduate student in the School of Physical Science Technology at ShanghaiTech University under the supervision of Prof. Zhijun Ning. He received his B.E. degree in Material Forming and Control Engineering in 2016. His research interests are on lead-free perovskite solar cells and quantum LED.

Wenjia Zhou is a postdoctoral fellow in the School of Physical Science and Technology at the ShanghaiTech University. He received his Ph.D. degree in Physics from the Institute of Physics, Chinese Academy of Sciences in 2015 and his Bachelor's degree in Material Chemistry from Sichuan University in China in 2009. His research interests include solar cells, photodetectors, and other optoelectronic devices from solution-processed semiconductors, such as colloidal quantum dots and perovskite.

Zhifang Shi is a Master degree candidate in the School of Physical Science Technology at ShanghaiTech University under the supervision of Prof. Qixi Mi. He received his B.S. degree in Applied Chemistry from Dalian University of Technology in 2014. His research interests include the design, crystal growth, and properties of perovskite materials.

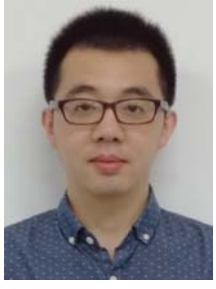

Binghan Li is a Ph.D. candidate in the School of Physical Science and Technology, ShanghaiTech University under the supervision of Prof. Qixi Mi. He received his B.E. degree in the School of Material Science and Engineering, Jiangsu University in 2013. His research interests involve perovskite solar cells, monocrystal photodetectors, and photocatalytic water splitting.

Prof. **Qixi Mi** earned his B.S. degree from Peking University in Applied Chemistry in 2003 and his Ph.D. degree from Northwestern University in Chemistry in 2009. Subsequently, he performed postdoctoral research at the California Institute of Technology, taking advantage of a fellowship of the NSF Center for Chemical Innovation (CCI Solar). He has been an assistant professor at the School of Physical Science and Technology of ShanghaiTech University since 2013. His main research topics include semiconducting photoelectrode materials, solar water splitting, photoelectron chemistry, as well as time-resolved optical spectroscopy and magnetic resonance.

Prof. **Zhijun Ning** received his Ph.D. degree at East China University of Science and Technology, under the supervision of Prof. He Tian. From 2009 to 2011, he worked as a postdoctoral scholar at the Royal Institute of Technology, Sweden. From 2011 to 2014, he was a postdoctoral scholar at the University of Toronto, under the supervision of Prof. Edward H. Sargent. In December 2014, he joined ShanghaiTech University as a faculty member. He is a recipient of the Young 1000 Talent Program. He has published more than 50 papers, and his work has been cited for over 4000 times. His research interests mainly include the synthesis and application of novel optoelectronic materials, such as nanocrystals and metal halide perovskite for solar cells, light-emitting diode, photodetectors, and photocatalysis.